PHYSICAL REVIEW B **79**, 155209 (2009)

Structural characterization of pressure-induced amorphous silicon

B. Haberl,[1,*] A. C. Y. Liu,[2,3] J. E. Bradby,[1] S. Ruffell,[1] J. S. Williams,[1] and P. Munroe[4]
[1]*Department of Electronic Materials Engineering, Research School of Physics and Engineering, The Australian National University, Canberra, Australian Capital Territory 0200, Australia*
[2]*Department of Materials Engineering, Monash University, Clayton, Victoria 3800, Australia*
[3]*Materials Science Division, Argonne National Laboratory, Argonne, Illinois 60439-4845, USA*
[4]*Electron Microscope Unit, University of New South Wales, Sydney, New South Wales 2052, Australia*
(Received 27 November 2008; revised manuscript received 4 March 2009; published 23 April 2009)

We investigate the structure and mechanical properties of pressure-induced (PI) amorphous silicon (*a*-Si) and compare this to the more extensively characterized case of *a*-Si created by ion implantation. To study the effect of thermal history we also examine the structure of both PI and ion-implanted *a*-Si after a low-temperature "relaxation" anneal (450 °C). Indentation testing suggests that structural changes are induced by thermal annealing. As-prepared forms of *a*-Si deform via plastic flow, while relaxed forms of *a*-Si transform to high-pressure crystalline phases. These structural changes are confirmed by more explicit measurements. Raman microspectroscopy shows that the short-range order as expressed by the average bond-angle distortion of the as-prepared amorphous phases is the same and reduced by the same amount following the low-temperature anneal. Fluctuation electron microscopy demonstrates that the as-prepared PI *a*-Si displays a much lower variance of the diffracted intensity, a feature directly correlated with the medium-range order, than the as-prepared ion-implanted *a*-Si. However, relaxation brings this variance of the two networks to the same intermediate level. The mechanical tests and structural probes indicate that annealing the amorphous silicon network can bring it to a common state with the same structure and properties regardless of the initial state. This final state might be the closest attainable to the continuous random network model.

DOI: 10.1103/PhysRevB.79.155209 PACS number(s): 61.05.J−, 61.43.Dq, 62.20.−x, 81.40.Gh

I. INTRODUCTION

The high-pressure behavior of a range of semiconductors has been extensively studied over the past 30 years and continues to be of wide interest.[1–6] It is well known that crystalline silicon (*c*-Si) undergoes a series of pressure-induced phase transformations. Both high-pressure diamond-anvil[1,3,4,7] and indentation experiments[5,8–11] have shown that the crystalline diamond-cubic Si-I phase transforms during loading at a pressure of ~11 GPa to the metallic β-Sn (Si-II) phase of Si, which is accompanied by a 22% increase in density. As Si-II is unstable at pressures below ~10 GPa,[3,4] the material undergoes further transformation on pressure release. Diamond-anvil experiments have shown the formation of the metastable high-pressure crystalline phases Si-XII (r8) and Si-III (bc8) on pressure release.[4] For indentation experiments, the final structure of the transformed volume can differ quite substantially from diamond-anvil results and depends critically on the unloading conditions, with slow unloading leading to the formation of a mixture of the high-pressure phases Si-XII and Si-III or a mixture of both these high-pressure phases and an amorphous silicon (*a*-Si) phase, but fast unloading leading to the sole formation of this *a*-Si phase.[10–12]

This pressure-induced (PI) form of *a*-Si is very interesting in its own right. Since its formation appears to be unique to the indentation process with its highly variable stress field under the indenter, the characterization of its structure may provide further insights into the dynamics of the pressure-induced phase transformation behavior of *c*-Si. Also, the characterization of this different form of *a*-Si might aid in better understanding the structural differences in *a*-Si networks prepared by different methods. To date, few attempts have been made to characterize the structure of PI *a*-Si. One study[13] found that the average interatomic distance depends on the unloading rates used to create the PI *a*-Si. The interatomic distance was found to be shorter if the PI *a*-Si was created directly from Si-II than if it was created with slower unloading rates in conjunction with the high-pressure phases Si-III and Si-XII.

An interesting feature of amorphous networks in general is that many of their properties depend on the thermal history and/or the preparation conditions. For example, when subjected to annealing, ion-implanted *a*-Si undergoes "structural relaxation" or short-range ordering.[14,15] This is the reduction in the number of coordination defects in the continuous random network (CRN) such that, for example, the average bond-angle distortion is decreased. Recently we have shown that these two states of *a*-Si, as-implanted and relaxed *a*-Si, show a very different behavior under indentation testing.[16] We found that the relaxed state undergoes a phase transformation to a metallic phase under loading and undergoes further phase transformations to the high-pressure phases Si-XII and Si-III under appropriate unloading conditions, whereas no evidence of phase transformation was found in the unrelaxed state of *a*-Si under low-load indentation. This different deformation behavior is also represented in the load-displacement curves, where the as-implanted case shows no discontinuity event upon unloading, while the relaxed case shows a clear "pop-out" event. Thus, indentation is a sensitive technique for probing the state of an amorphous network.

The aim of our current study was to investigate the structure and properties of PI *a*-Si. These investigations were carried out as a function of thermal history to examine whether

 ©2009 The American Physical Society

PI a-Si undergoes structural relaxation similar to ion-implanted a-Si. Hence, the mechanical properties were characterized using nanoindentation. Raman microspectroscopy and cross-sectional transmission electron microscopy (XTEM) were used to probe for the formation of new pressure-induced phases from the mechanical tests. Raman microspectroscopy was also employed to characterize the short-range order (SRO) parameters of the amorphous networks, or ordering within the first-coordination shell and below 1 nm. Fluctuation electron microscopy (FEM) was used to examine structural order at longer length scales, in the realm of medium-range order (MRO), which can be defined as order on the scale of $\sim 1-3$ nm. To provide a reference, we examined the more extensively studied material of a-Si created by ion implantation with the same techniques.[14–19]

II. EXPERIMENTAL

PI a-Si was formed using an Ultra-micro indentation system 2000 (UMIS) with a spherical diamond indenter of ~ 18 μm radius at room temperature and ambient pressure. Large arrays of 8×8 indentations were performed on single crystal Cz Si(100), p-doped with boron to a resistivity of $10-20$ Ω cm. Loads of up to 700 mN were applied at an average loading rate of ~ 5 mN/s and unloading was performed within less than 1 s. This resulted in a transformed zone of PI a-Si of ~ 9 μm diameter and extending ~ 400 nm below the surface. The loading conditions used ensured that no cracking occurred and that the formation of a-Si was much more likely on unloading than the formation of Si-XII/Si-III. Raman microspectroscopy was used to confirm that no crystalline high-pressure phases were present within each residual indent, at least to the extent of the sensitivity of the Raman technique. For the FEM study, loads up to 750 mN were applied at a loading rate of 5 mN/s, and a fast unloading rate was employed with unloading occurring within 1 s. In this case, cracking was observed occasionally around the residual indent impressions.

For the ion-implanted a-Si samples, a continuous 2-μm-thick surface amorphous layer was created by multiple implantations of Si ions at energies of 80 keV, 500 keV, 1 MeV, 1.5 MeV, and 2 MeV into single-crystal Si angled at 7° relative to the incident beam. The implantation was performed at liquid-nitrogen temperature using the ANU 1.7 MV NEC tandem high-energy ion implanter. The fluence for each energy was 1×10^{15} cm^{-2}. Relaxation anneals were performed on half of both the as-indented PI a-Si samples and as-implanted ion-implanted a-Si samples. This furnace annealing was conducted at 450 °C for 30 min in a nitrogen atmosphere.

Mechanical testing was conducted on the various a-Si forms using a Hysitron TriboIndenter with a diamond Berkovich indenter. Loads up to 5 mN were applied using a loading time of 30 s and an unloading time of 60 s. These indentation conditions resulted in a maximum penetration depth of ~ 130 nm and a "radius" of the residual indent of ~ 500 nm. Precise positioning achieved by scanning across the surface with the indentation tip ensured that the mechanical testing was performed in the center of the transformed zones. Thus, the reindentation process in the PI a-Si was not influenced by the surrounding c-Si as the entire process was completely surrounded by previously transformed material (~ 4 μm laterally and ~ 200 nm in depth). Henceforth the larger residual indents made by the UMIS will be referred to as microindents, while those made by the Hysitron TriboIndenter as nanoindents.

Raman microspectroscopy was conducted with a Renishaw 2000 Raman imaging microscope using the 632.8 nm excitation line of a helium-neon laser with an incident power of 2.10 mW focused to a spot of ~ 1.0 μm radius. A good spectrum was usually obtained after only one accumulation of 30 s. Under these testing conditions repeated measurements in the same area confirmed that the a-Si was unaltered by the measurement.

Selected nanoindents in PI a-Si samples were prepared for XTEM using an FEI xT Nova NanoLab 200. Prior to loading the samples into the focused ion beam (FIB) system, an ~ 50 nm layer of gold was sputtered onto the surface to protect the top surface of the samples from any implantation-induced damage. In addition, an ~ 1 μm platinum layer was deposited on top of the gold-coated surface using the FIB system to shield the sample from damage during the ion-milling process. A Philips CM 300 operating at an accelerating voltage of 300 kV was used for the conventional bright-field TEM imaging.

Plan-view specimens of all four types of a-Si were prepared for FEM. This was done by first-making specimens of 3 mm diameter from both ion-implanted a-Si and c-Si samples using a Gatan ultrasonic disk cutter 601. Indentation using the UMIS was then performed in the middle of the 3 mm diameter c-Si samples to make PI a-Si. Some of the ion-implanted a-Si disks and some of the c-Si disks containing PI a-Si were annealed to relax the amorphous network as described above. All samples were dimpled to a thickness of ~ 10 μm using a Gatan dimple grinder 656 and then further thinned by wet etching to electron transparency using HNO_3:HF:CH_3COOH in a ratio of 5:1:1.

A Jeol JEM-4000EXII located at Argonne National Laboratory was used for the FEM study. The instrument was operated at 200 keV to avoid damage by the electron beam. The FEM consisted of the automated acquisition of a series of tilted dark-field images at different incident beam tilts. The hollow cone dark-field TEM technique that is more commonly employed for FEM is the incoherent azimuthal average of the tilted dark-field technique and probes essentially the same structural information.[20,21] The images were filtered to remove distortions and noise and the normalized intensity variance was calculated.[20] This quantity is a function of the pair-pair correlation functions in the material[21] and hence is sensitive to both the degree and type of the MRO in the material. The size of the objective aperture dictates a sensitivity to MRO up to 1.2 nm in extent. We present the intensity variance as a function of the incident beam tilt projected onto the diffraction plane, k (nm^{-1}). The size of the dark-field images was of 250×250 nm^2. To avoid thickness effects,[20] only areas of a uniform thickness of ~ 50 nm were studied in all specimens. This thickness was estimated and controlled by measuring the normalized bright-field image intensity.[20] Approximately ten dark-field series were obtained

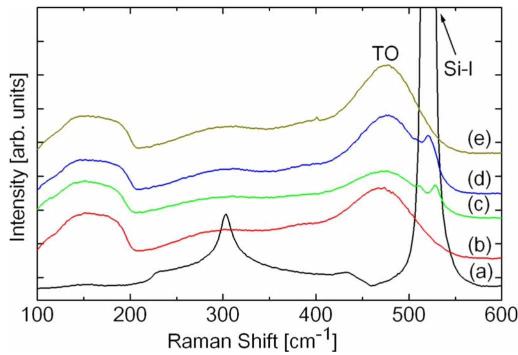

FIG. 1. (Color online) Raman spectra of (a) pristine *c*-Si, (b) as-implanted *a*-Si, (c) as-indented PI *a*-Si, (d) relaxed PI *a*-Si, and (e) relaxed ion-implanted *a*-Si. The microindents were made in *c*-Si with the UMIS using an ~18 μm indenter loading up to 700 mN and unloading within ~1 s.

from different areas of each specimen. The displayed FEM data are the average of ten measurements and the uncertainty is the standard error.

III. RESULTS

A. Raman microspectroscopy

Raman microspectroscopy is not only sensitive to different crystalline structures but also very sensitive to the SRO of an amorphous network. It has been shown that the characteristics of the broad transverse-optic (TO)-like peak at approximately 480 cm^{-1} are correlated with SRO and thus the peak width (Γ_{TO}) indicates whether the state of *a*-Si is relaxed or unrelaxed.[15,17] Moreover, Γ_{TO} has a simple empirical relation to the average bond-angle distortion ($\Delta\theta$) within the CRN,[15,17,22] with a lower peak width correlating to a lower $\Delta\theta$.

The Raman spectra for as prepared and relaxed ion implanted and PI *a*-Si are shown in Fig. 1. A spectrum for pristine *c*-Si is also shown for comparison. All the forms of amorphous silicon studied here have Raman features typical of *a*-Si, namely, the broad TO-like peak at approximately 480 cm^{-1} as marked in Fig. 1. The Raman spectra of the as-indented PI *a*-Si and, less visible, of the relaxed PI possess additional peaks at 511 and 529 cm^{-1}, thought to originate from residual stresses in the underlying *c*-Si, a topic that will be explored in depth elsewhere.[23]

To analyze the SRO, the TO-like peak half-width ($\Gamma_{TO}/2$) was determined for each type of *a*-Si. $\Gamma_{TO}/2$ is used rather than Γ_{TO} in order to compare our results with those from previous studies.[15,17] The TO-like peak was fitted with a Gaussian using the package ORIGIN.[24] Care was taken to avoid effects caused by an overlap of the TO-like peak on the low wave-number side with other features in all cases of *a*-Si, and in the case of PI *a*-Si, interference with the additional Si-I peaks on the high wave-number side. $\Delta\theta$ was calculated according to the empirical rule derived from model calculations by Beeman *et al.*[22] and is summarized together with $\Gamma_{TO}/2$ for each case in Table I. The error in $\Gamma_{TO}/2$ is caused by the intrinsic error of the Raman system plus uncertainties from the fitting procedure.

TABLE I. Comparison of $\Gamma_{TO}/2$ and $\Delta\theta$ of as-implanted and relaxed ion-implanted *a*-Si and as-indented and relaxed PI *a*-Si.

Form of *a*-Si	$\Gamma_{TO}/2$ (cm^{-1})	$\Delta\theta$ (deg)
As-implanted	40 ± 2	10.8 ± 0.5
Relaxed implanted	33 ± 2	8.5 ± 0.5
As-indented PI	41 ± 2	11.2 ± 0.5
Relaxed PI	35 ± 2	9.2 ± 0.5

In the case of ion-implanted *a*-Si $\Gamma_{TO}/2$ was decreased by 18% after annealing, which is typical for the difference between as-implanted and relaxed implanted *a*-Si.[15,17] In the case of PI *a*-Si, $\Gamma_{TO}/2$ also decreased by 15% after annealing. It appears that $\Delta\theta$ is similar for the two as-prepared cases which might suggest a similar SRO. Furthermore, the $\Gamma_{TO}/2$ and $\Delta\theta$ values of both relaxed ion-implanted and relaxed PI *a*-Si are the same within the error, suggesting that the SRO in the relaxed state of both forms of *a*-Si is the same.

B. Mechanical testing using nanoindentation

Examples of the load-displacement curves of nanoindents made in the middle of the large residual microindents are shown in Fig. 2. The resulting shapes of the unloading curves differ significantly for nanoindents made in relaxed and as-indented microindents. We note that the unloading rate used was slow enough to form crystalline high-pressure phases if Si-II was formed during loading. While the load-displacement curve of a nanoindent in the relaxed PI *a*-Si shows clearly a pop-out event, the one in as-indented PI *a*-Si does not display any such event. This pop-out event is a clear

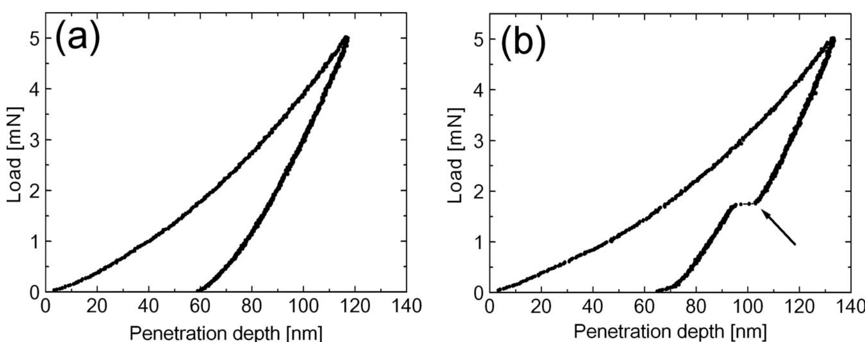

FIG. 2. Load-displacement curves of nanoindents in (a) as-indented and (b) relaxed PI *a*-Si. In the latter case a pop-out event is indicated by the arrow. The indentation was performed by loading to 5 mN within 30 s and unloading within 60 s.

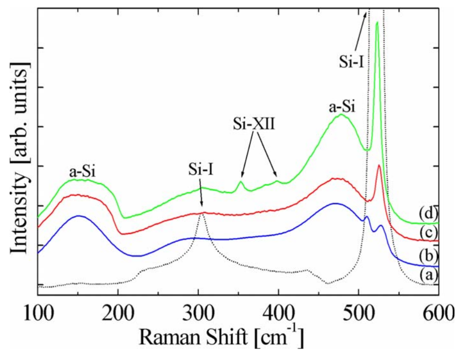

FIG. 3. (Color online) Raman spectra of (a) pristine *c*-Si, (b) as-indented PI *a*-Si, (c) nanoindented as-indented PI *a*-Si, and (d) nanoindented relaxed PI *a*-Si. The nanoindentation was performed with the Hysitron using a Berkovich tip loading up to 5 mN within 30 s and unloading within 60 s.

indication of a pressure-induced phase transformation and the formation of high-pressure phases on unloading, while the smooth unloading curve in the as-indented case suggests deformation via plastic flow.[16] Additionally, we note that the maximum and the residual penetration depths in the as-indented case are approximately 10% less than in the relaxed case, which might indicate, somewhat surprisingly and contrary to ion-implanted *a*-Si,[18,19] a higher hardness of the as-indented PI *a*-Si over relaxed PI *a*-Si.

Raman microspectroscopy was used to investigate the possible formation of pressure-induced phases during the mechanical tests, as shown in Fig. 3. No difference in the Raman spectra were observed after reindentation of as-indented PI *a*-Si. However, additional bands at 350 and 395 cm^{-1} appeared after reindentation of relaxed PI *a*-Si. Such bands can be attributed to the presence of Si-XII.[9,11]

The occurrence of phase transformations was further investigated by XTEM of residual nanoindents in as-indented and relaxed PI *a*-Si. The nonpyramidal shape of the residual nanoindents is due in some degree to the blunting of the Berkovich tip after scanning across the microindents prior to reindentation. Figure 4(a) shows a bright-field image of a whole microindent of as-indented PI *a*-Si, while Fig. 4(b) shows a closeup of the residual nanoindent. Consistent with the load-displacement curves and the Raman data there is no evidence of transformation. No crystalline phases are visible below the nanoindent, strongly suggesting deformation via plastic flow. However, the situation is different when looking at a residual nanoindent made in relaxed PI *a*-Si. The whole microindent is displayed in Fig. 5(a), while again a closeup of the nanoindent made in relaxed PI *a*-Si is shown in Fig. 5(b). As indicated by an arrow, small grains from crystallites are clearly seen, with a contrast that differs substantially from that of the amorphous phase. However, due to the very small size and random orientation of these crystallites it was not possible to obtain a good diffraction pattern. This was further complicated by the fact that the small crystallites appeared to anneal out under the electron beam. Nonetheless, the presence of crystalline material beneath the residual nanoindent is clearly confirmed and Raman microspectroscopy has indicated that the residual nanoindent contains the high-pressure phase Si-XII.

C. Fluctuation electron microscopy

FEM measures the variance in the diffracted intensity in contrast to the average in diffracted intensity that is measured by diffraction techniques. Measuring the second moment in the scattered intensity distribution gives FEM access to pair-pair atomic correlation functions and hence sensitivity to order beyond first-neighbor distances and in the realm of MRO. To date, for the case of amorphous semiconductors the magnitude of the variance has been correlated with the degree of MRO by interpreting a higher variance as indicative of a higher degree of MRO.[25–28] This degree of MRO depends on a number of indistinguishable factors such as the number of regions of correlated structure, the size of these regions, and the relative order within such a region. Moreover, the positions of the peaks in the variance plot give some additional insight into the local bonding and the type of MRO within the regions of correlated structure.[20,21] However, a unique determination of the atomic arrangements that give rise to the features in the variance plot is difficult and requires extensive atomic modeling. Nevertheless, relative differences between different *a*-Si samples can illuminate many details of the structure as we see below. Our averaged FEM data for the different forms of *a*-Si are shown in Fig. 6. Individual plots were fitted by three Gaussians using the

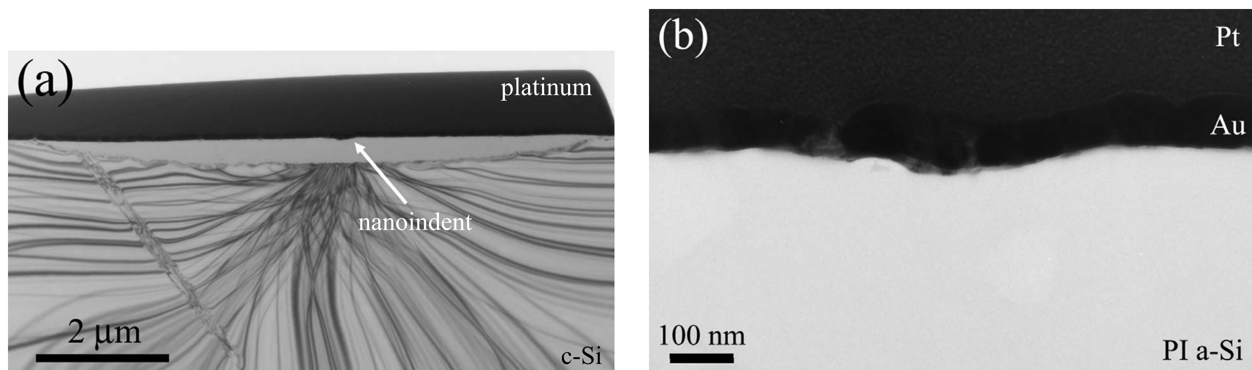

FIG. 4. XTEM of (a) a microindent with a nanoindent in as-indented PI *a*-Si and of (b) the respective nanoindent. The nanoindentation was performed with the Hysitron using a Berkovich tip loading up to 5 mN within 30 s and unloading within 60 s.

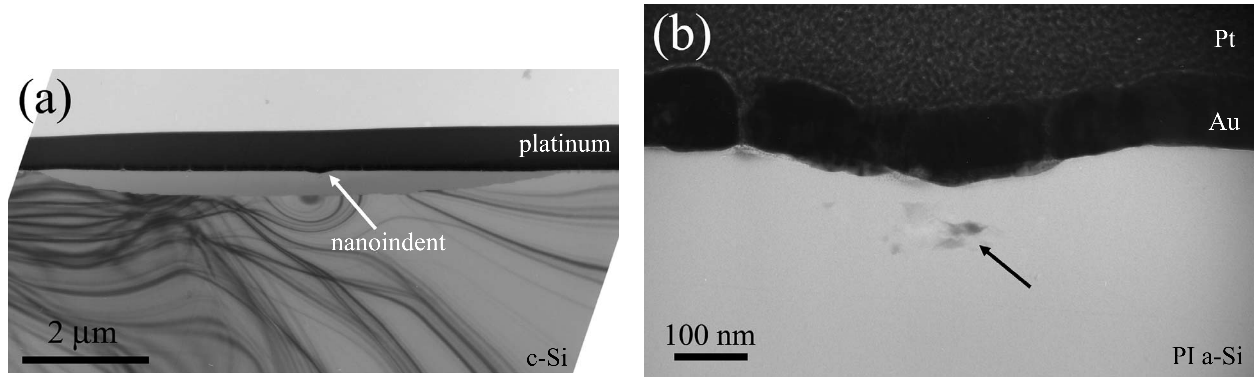

FIG. 5. XTEM of (a) a microindent with a nanoindent in relaxed PI *a*-Si and of (b) the respective nanoindent. The nanoindentation was performed with the Hysitron using a Berkovich tip loading up to 5 mN within 30 s and unloading within 60 s.

package ORIGIN.[24] The average peak positions quoted with standard error are summarized in Table II. In the case of ion-implanted *a*-Si, relaxation decreases the intensity variance and also results in a significant downshift in peak position. In contrast, as-indented PI *a*-Si has the lowest initial intensity variance. Relaxation increases this variance significantly, and a similar downshift in peak position is observed. It is significant that the MRO in the relaxed films (both PI and ion implanted) is essentially identical, with both networks displaying the same peak magnitudes and positions.

IV. DISCUSSION

Measurements on as-prepared ion-implanted and PI *a*-Si as well as on their relaxed forms show intriguing differences and similarities. For example, the as-prepared forms show markedly different MRO although some similarities are observed in their modes of mechanical deformation and SRO. In contrast, the relaxed states of both forms of *a*-Si exhibit remarkably similar properties.

Before considering the different amorphous networks in detail, let us comment on the role of hydrogen diffusion into *a*-Si during thermal annealing. After the thermal anneal at 450 °C the concentration of hydrogen in relaxed ion-implanted *a*-Si ranges from around 7×10^{19} cm^{-3} on the top surface to around 1×10^{17} cm^{-3} at a depth of 400 nm as measured by secondary ion mass spectrometry (not shown here). The hydrogen concentration in as-implanted *a*-Si is below the sensitivity limit of the experimental setup but is presumed to be similar to the equilibrium concentration of hydrogen in *c*-Si (Ref. 29) of around 1×10^{12} cm^{-3} since no in-diffusion is expected to occur at room temperature.[30] The concentrations will be the same for relaxed and as-indented PI *a*-Si, respectively, as they are also created from *c*-Si and, in the case of relaxed PI *a*-Si, annealed in the same way. One might argue that this hydrogen in-diffusion might be responsible for the change in the amorphous network upon annealing rather than an intrinsic change to the structure. Indeed, a decrease in the variance intensity obtained from FEM has been reported for hydrogen diffusion into certain types of magnetron sputtered *a*-Si (Ref. 31 and references therein). These films, however, contained around 15% hydrogen before the in-diffusion, a concentration that is not only much higher than the observed concentration in our films but also even higher than the solubility limit of hydrogen in ion-implanted *a*-Si (3%–4%).[32] Additionally, no downshift in peak position was observed in this case, which suggests a different change to the amorphous network than caused by thermal annealing. Moreover, in a previous study it was observed that (hydrogenated) plasma-enhanced chemical-vapor deposition grown *a*-Si did not phase transform but always deformed via plastic flow.[33] Thus, hydrogenated amorphous networks seem to be structurally different from the relaxed *a*-Si networks studied here as both relaxed forms of *a*-Si clearly phase transform. Therefore, we believe that the diffusion of hydrogen during annealing does not play a significant role for the changes in the amorphous networks reported here.

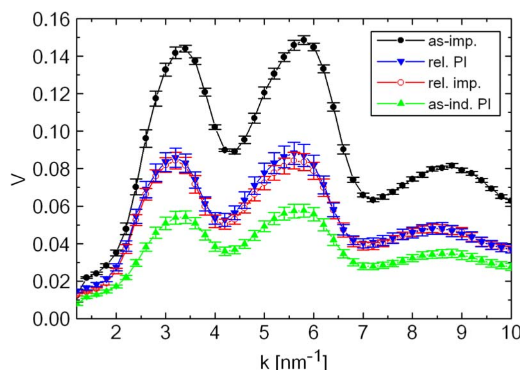

FIG. 6. (Color online) Variance as a function of *k* for as-implanted, relaxed implanted, as-indented, and relaxed PI *a*-Si.

TABLE II. Peak positions in the $V(k)$ plots of the different forms of *a*-Si from Gaussian fits to the data.

Form of *a*-Si	Peak 1 (nm^{-1})	Peak 2 (nm^{-1})	Peak 3 (nm^{-1})
As-implanted	3.28 ± 0.03	5.63 ± 0.03	8.79 ± 0.03
Relaxed Implanted	3.11 ± 0.03	5.47 ± 0.03	8.64 ± 0.02
As-indented PI	3.26 ± 0.02	5.57 ± 0.02	8.73 ± 0.02
Relaxed PI	3.12 ± 0.02	5.46 ± 0.03	8.63 ± 0.02

Let us now consider the as-prepared states in detail first. Indentation using the loading conditions studied here indicates that both as-prepared materials deform via plastic flow without any evidence of phase transformations; i.e., the deformation behavior is essentially the same in both forms of *a*-Si. This, however, is in marked contrast to the relaxed forms of *a*-Si, which transform to high-pressure crystalline phases on indentation. Interestingly, from the mechanical tests it seems that the two as-prepared samples differ in hardness, with the as-indented PI *a*-Si displaying a higher hardness than the as-implanted *a*-Si. However, we note, that hardness is not a true materials property but rather the "resistance" of the material to deformation by the indenter tip. Thus, the increased hardness of as-indented PI *a*-Si compared to ion-implanted *a*-Si might be a consequence of a higher mass density of PI *a*-Si which arises from the transformation of a high-density metallic form of silicon to much less dense *a*-Si during unloading.

In addition to similar deformation behavior, estimations of the average bond-angle distortion from Raman microspectroscopy indicate that the as-prepared *a*-Si types have a similar SRO. This result is also consistent with the similarity in peak positions in the FEM data which are evidence for similar average local bonding. In the case of as-implanted *a*-Si the observed higher average bond-angle distortion has been linked to the presence of point defects or point-defect complexes and a high dangling-bond density,[15] which leads to an imperfect CRN. Previously, we have discussed that this high defect or dangling-bond density may aid material flow by facilitating propagation of defects or dangling bonds.[34] Thus, the similar SRO and deformation behavior of as-indented PI *a*-Si could suggest similarly disordered material. However, the increased hardness value of as-indented PI *a*-Si over as-implanted *a*-Si might indicate more complex structural differences.

Intriguingly, the degree of MRO, as expressed by the variance differences in the FEM plot, differs markedly between the as-prepared films, with the as-indented PI *a*-Si displaying a much lower variance than the as-implanted *a*-Si case. These differences clearly reflect structural differences, which presumably arise from the dramatically different preparation method: one formed from ion disordering of crystalline Si and the other from the transformation of a metastable high-pressure phase (Si-II). The nature of such structural differences is not easy to ascertain, as a result of the difficulty in interpreting differences in MRO data obtained from FEM. Even more difficult is to understand how such differences relate to structure. Since FEM data do not directly allow a unique model of the amorphous structure to be constructed, previous studies have inferred structural information from FEM data by comparing the measured variance with simulations from proposed models. For deposited *a*-Si, and also to some extent for ion-implanted *a*-Si, two distinct models have been proposed: a paracrystalline model[21,26,27,35,36] and a void model.[37,38] However, both the paracrystalline and the void model were found to fit the data equally well, demonstrating the essential nonuniqueness of structural models obtained by a particular solution to the FEM data. Furthermore, the paracrystalline model for ion-implanted *a*-Si is somewhat controversial.[39] Thus, the precise nature of structural differences cannot be determined in detail from the experimental results presented here. Nonetheless, it is possible to gain some insight into possible structural differences by examining how FEM variance data arises and comparing FEM observations with other (known) properties of PI and ion-implanted *a*-Si.

FEM measures the variance in the diffracted intensity, in our case the variance in the speckle pattern of the collected dark-field images. These speckles are thought to be caused by the diffraction contrast of small regions containing correlated atomic arrangements. Thus, a completely random alignment of atoms is expected to give rise to a dark-field image without significant "speckliness" (i.e., low variance). However, an example of the difficulties in interpreting the intensity variance from FEM has been demonstrated by the phenomenological modeling of Stratton and Voyles.[28] Their model shows that for sparsely distributed nanocrystallites in an amorphous matrix the magnitude of the intensity variance will increase with increasing number and size of the nanocrystallites. However, once a threshold in volume fraction is surpassed, increasing numbers of nanocrystallites will act to increase the homogeneity and so reduce the intensity variance. While this model has been developed for perfect nanocrystallites, one might expect similar principles to also hold true for other noncrystalline but correlated atomic arrangements. However, in the case of amorphous silicon, Stratton and Voyles[28] noted that the volume fraction of correlated regions seems to be sparse enough to allow the interpretation that a higher intensity variance implies increased spatial heterogeneity and thus a higher degree of MRO. Therefore, this interpretation will be employed throughout this article.

To gain further insights into the observed difference in intensity variance let us consider how the different formation processes of the different forms of *a*-Si studied here might contribute to the rise of speckles in a dark-field image. Ion-implanted *a*-Si and the disordering that leads to it arises from the sum of individual collision cascades caused by the implanted energetic Si ions,[40] a process which can clearly result in an inhomogeneous amorphous network. For example, within a collision cascade, the atomic motion can be considered as a displacement cascade or thermal spike. In the latter case local melting and quenching can occur on a time scale on the order of 10^{-15} s. Both types of collision spike can lead to bonding defects and density variations across the cascade. Furthermore, the length scale of the damage surrounding such a Si-ion collision cascade is slightly larger or on the order of the length scale of the MRO (variance in the speckle pattern) probed for here (1.2 nm). Thus, FEM is very likely to be sensitive to the inhomogeneities in *a*-Si generated by collisional processes of ion implantation. Such inhomogeneities may consist, for example, of localized changes in mass density between the edges and the core of the cascades, "defectlike" differences or differences in residual strain. Defectlike differences could be differences in the ratio of so-called five- and seven-membered rings[41] within the amorphous network at different parts of the residual cascade volumes. These locally heterogeneous regions might have different atomic (bonding) arrangements and thus differences in local diffraction contrast might be expected to occur. These differences may appear as speckles on the dark-field image, yield-

ing a larger intensity variance than a homogenous medium of the same average density. This situation, however, is very different to the case of as-indented PI *a*-Si. The clear differences observed in hardness, along with our preliminary mass-density measurements by electron-energy-loss spectroscopy (not shown here) suggest that as-indented PI *a*-Si has a higher (average) density than relaxed *a*-Si and even *c*-Si, while as-implanted *a*-Si (and also relaxed implanted *a*-Si) are slightly less dense than *c*-Si.[42] This lower mass density of as-implanted *a*-Si may facilitate local atomic structural differences in the as-implanted network compared with the denser network of the as-indented PI *a*-Si. Conversely, the denser amorphous network of the as-indented PI *a*-Si may constrain local structural differences giving rise to greater homogeneity, a reduced speckliness in the dark-field image and hence a measured low variance in the FEM data. For example, defectlike differences such as local changes in the ratio of five- and seven-membered rings may be small as a result of a higher average density and associated constraints on atomic arrangements. Moreover, the creation of PI *a*-Si by the simultaneous transformation of large volumes of material might also give rise to a greater homogeneity of the amorphous network. However, one has to be cautious when interpreting the network of the as-indented PI *a*-Si as homogeneous over the whole volume of the transformed zone since its properties have only been studied by the use of plan-view samples, which probe the top (near-surface) region of the PI amorphous zone. Thus, it could be quite possible that a difference in intensity variance (and other properties) would be observed between the top and bottom layers of the transformed zone.

Let us now turn our attention to both relaxed forms of *a*-Si. The mechanical tests of relaxed PI *a*-Si reveal the same deformation behavior as for relaxed ion-implanted *a*-Si.[16] Both relaxed cases clearly phase transform under pressure as confirmed by Raman microspectroscopy and by XTEM of residual nanoindents. Despite the similarity in mechanical deformation of both forms of *a*-Si after relaxation, it is interesting that PI *a*-Si decreases in hardness after annealing, whereas ion-implanted *a*-Si increases by a small amount on annealing. However, in the case of relaxed ion-implanted or PI *a*-Si, the hardness is defined by the onset of an *a*-Si to Si-II phase transformation, while in the case of the as-prepared forms of *a*-Si it appears to be governed by their ability to flow plastically. This fact complicates the comparison of the hardness of a phase transforming and a nonphase transforming material considerably.

It is also interesting that the SRO and MRO of both relaxed amorphous silicon networks are identical within the sensitivity of our techniques. Raman microspectroscopy shows that annealing increases the SRO of PI *a*-Si similar to that for ion-implanted *a*-Si,[15,17] resulting in the same reduction in the average bond-angle distortion. Additionally, both films exhibit the same average bond-angle distortion after the relaxation anneal. FEM reveals that both relaxed cases display not only the same intensity variance but also the same type of MRO, as evident from an identical and significant downshift in peak position, regardless of the as-prepared starting state. The reason that a significant intensity variance is observed for relaxed *a*-Si may relate to the facilitation of local five- and seven-membered ring ratio variations as a result of low density of the random atomic arrangement. This effect could give rise to an appreciable speckliness in the collected dark-field images. The lowering of the intensity variance upon annealing of the ion-implanted *a*-Si has been reported before, but the shift in the peak position has not.[27] Previously, this lower variance of annealed specimens has been attributed to the approach to a more ideal CRN for not only ion-implanted *a*-Si,[27] but also for amorphous germanium.[25] Thus, our observations not only suggest that relaxed PI *a*-Si is, within the sensitivity of our techniques, the same as relaxed ion-implanted *a*-Si, but also that this relaxed state of *a*-Si may be as close to the CRN model as is practically possible.

The structural relaxation or short range ordering of ion-implanted *a*-Si has been linked, from calorimetry measurements, to the annihilation of point defects and point-defect complexes.[15] While these defect concentrations lead to a distortion of bond angles and an accompanying strain field, their annihilation yields a more ideal CRN due to the reduction in the average bond-angle distortion. From our studies, relaxation of both PI and ion-implanted *a*-Si forms induces short range ordering by minimizing the average bond-angle distortion and presumably also by the annealing of "defects" within the amorphous network. In addition, relaxation also involves either a decrease or an increase in the intensity variance, depending on the starting structure of the amorphous network. We infer from hardness measurements that relaxation may also involve significant changes to the mass density, with the direction of change again depending on the starting state of the material. Such observations underscore the subtle structural differences between amorphous networks with exactly the same composition but different histories.

Finally, although this study has highlighted structural differences that are dependent on the starting form of *a*-Si and a tendency for relaxation to result in a single state indicative of an ideal CRN, clearly more detailed measurements are needed to fully understand the differences in the initial structures. We are currently undertaking precise measurements of the mass density, pair-distribution function using electron diffraction, and hardness of these same samples and anticipate that the results of these studies will contribute to the resolution of such issues. In terms of relaxation of different starting forms of *a*-Si, it will also be instructive to establish whether other forms of *a*-Si such as laser-quenched material or ultrahigh-vacuum deposited *a*-Si relax to a similar state with similar SRO and MRO.

V. CONCLUSION

The structure of as-indented and relaxed PI *a*-Si has been investigated in some detail and compared to as-implanted and relaxed ion-implanted *a*-Si. It has been shown that both as-prepared forms of *a*-Si deform via plastic flow under mechanical testing and share the same SRO. However, despite these similarities, the intensity variance displayed by the as-implanted *a*-Si and the as-indented PI *a*-Si forms differ markedly. This different variance reflects clear differences in

preparation history: one formed by ion disordering of crystalline Si and the other from a transformation from a metallic high-pressure phase (Si-II).

Intriguingly, relaxation of both forms of *a*-Si appears to result in the same SRO with minimal average bond-angle distortion, the same MRO and indeed almost the same mechanical (transformation) behavior. This behavior indicates that thermal relaxation of impurity-free *a*-Si leads to the same amorphous state regardless of the preparation technique and starting structure. Furthermore, this suggests strongly that relaxed *a*-Si approaches a more equilibrium state of pure *a*-Si and might be the closest attainable state to the CRN model.

ACKNOWLEDGMENTS

The authors would like to acknowledge and thank N. J. Zaluzec and R. E. Cook of the Materials Science Division at Argonne National Laboratory for the assistance during the collection of preliminary diffraction data. Funding provided by the Australian Research Council is gratefully acknowledged. The electron microscopy was accomplished at the Electron Microscopy Center for Materials Research at Argonne National Laboratory, a U.S. Department of Energy Office of Science Laboratory operated under Contract No. DE-AC02-06CH11357 by UChicago Argonne, LLC.

*bxh109@rsphysse.anu.edu.au

[1] S. Minomura and H. G. Drickamer, J. Phys. Chem. Solids **23**, 451 (1962).

[2] A. P. Gerk and D. Tabor, Nature (London) **271**, 732 (1978).

[3] J. Z. Hu, L. D. Merkle, C. S. Menoni, and I. L. Spain, Phys. Rev. B **34**, 4679 (1986).

[4] R. O. Piltz, J. R. Maclean, S. J. Clark, G. J. Ackland, P. D. Hatton, and J. Crain, Phys. Rev. B **52**, 4072 (1995).

[5] J. E. Bradby, J. S. Williams, and M. V. Swain, Phys. Rev. B **67**, 085205 (2003).

[6] P. F. McMillan, M. Wilson, D. Daisenberger, and D. Machon, Nat. Mater. **4**, 680 (2005).

[7] M. Imai, T. Mitamura, K. Yaoita, and K. Tsuji, High Press. Res. **15**, 167 (1996).

[8] G. M. Pharr, W. C. Oliver, R. F. Cook, P. D. Kirchner, M. C. Kroll, T. R. Dinger, and D. R. Clarke, J. Mater. Res. **7**, 961 (1992).

[9] Y. Gogotsi, C. Baek, and F. Kirscht, Semicond. Sci. Technol. **14**, 936 (1999).

[10] V. Domnich, Y. Gogotsi, and S. Dub, Appl. Phys. Lett. **76**, 2214 (2000).

[11] J. E. Bradby, J. S. Williams, J. Wong-Leung, M. V. Swain, and P. Munroe, J. Mater. Res. **16**, 1500 (2001).

[12] D. R. Clarke, M. C. Kroll, P. D. Kirchner, R. F. Cook, and B. J. Hockey, Phys. Rev. Lett. **60**, 2156 (1988).

[13] I. Zarudi, J. Zhou, W. McBride, and L. C. Zhang, Appl. Phys. Lett. **85**, 932 (2004).

[14] S. Roorda, S. Doorn, W. C. Sinke, P. M. L. O. Scholte, and E. van Loenen, Phys. Rev. Lett. **62**, 1880 (1989).

[15] S. Roorda, W. C. Sinke, J. M. Poate, D. C. Jacobson, S. Dierker, B. S. Dennis, D. J. Eaglesham, F. Spaepen, and P. Fuoss, Phys. Rev. B **44**, 3702 (1991).

[16] B. Haberl, J. E. Bradby, S. Ruffell, J. S. Williams, and P. Munroe, J. Appl. Phys. **100**, 013520 (2006).

[17] S. Roorda, J. M. Poate, D. Jacobson, B. S. Dennis, S. Dierker, and W. Sinke, Appl. Phys. Lett. **56**, 2097 (1990).

[18] J. S. Williams, J. S. Field, and M. V. Swain, *Thin Films: Stresses and Mechanical Properties IV*, MRS Symposia Proceedings No. 308 (Materials Research Society, Pittsburgh, 1993), p. 571.

[19] D. M. Follstaedt, J. A. Knapp, and S. M. Myers, J. Mater. Res. **19**, 338 (2004).

[20] A. C. Y. Liu, R. Arenal, D. J. Miller, X. Chen, J. A. Johnson, O. L. Eryilmaz, A. Erdemir, and J. B. Woodford, Phys. Rev. B **75**, 205402 (2007).

[21] M. M. J. Treacy, J. M. Gibson, L. Fan, D. J. Paterson, and I. McNulty, Rep. Prog. Phys. **68**, 2899 (2005).

[22] D. Beeman, R. Tsu, and M. F. Thorpe, Phys. Rev. B **32**, 874 (1985).

[23] B. Haberl, J. E. Bradby, and J. S. Williams (unpublished).

[24] Microcal Origin Version 6.0 (Microcal Software, Northampton, MA, 1999).

[25] J. M. Gibson and M. M. J. Treacy, Phys. Rev. Lett. **78**, 1074 (1997).

[26] M. M. J. Treacy, J. M. Gibson, and P. J. Keblinski, J. Non-Cryst. Solids **231**, 99 (1998).

[27] J.-Y. Cheng, J. M. Gibson, P. M. Baldo, and B. J. Kesel, J. Vac. Sci. Technol. A **20**, 1855 (2002).

[28] W. G. Stratton and P. M. Voyles, Ultramicroscopy **108**, 727 (2008).

[29] S. J. Pearton, J. W. Corbett, and J. T. Borenstein, Physica B (Amsterdam) **170**, 85 (1991).

[30] G. L. Olson and J. A. Roth, in *Handbook of Crystal Growth 3*, edited by D. T. J. Hurle (Elsevier, New York, 1994).

[31] L. N. Nittala, S. Jayaraman, B. A. Sperling, and J. R. Abelson, Appl. Phys. Lett. **87**, 241915 (2005).

[32] S. Acco, D. L. Williamson, P. A. Stolk, F. W. Saris, M. J. van den Boogaard, W. C. Sinke, W. F. van der Weg, S. Roorda, and P. C. Zalm, Phys. Rev. B **53**, 4415 (1996).

[33] J. S. Williams, B. Haberl, and J. E. Bradby, *Fundamentals of Nanoindentation and Nanotribology III*, MRS Symposia Proceedings No. 841 (Materials Research Society, Pittsburgh, 2005), p. R10.3.1/T6.3.1.

[34] B. Haberl, J. E. Bradby, M. V. Swain, J. S. Williams, and P. Munroe, Appl. Phys. Lett. **85**, 5559 (2004).

[35] P. M. Voyles, Ph.D. thesis, University of Illinois at Urbana-Champaign, 2001.

[36] P. M. Voyles and J. Abelson, Sol. Energy Mater. Sol. Cells **78**, 85 (2003).

[37] P. Biswas, D. N. Tafen, R. Atta-Fynn, and D. Drabold, J. Phys.: Condens. Matter **16**, S5173 (2004).

[38] P. Biswas, R. Atta-Fynn, S. Chakraborty, and D. A. Drabold, J. Phys.: Condens. Matter **19**, 455202 (2007).

[39] S. Roorda, J. Vac. Sci. Technol. A **21**, 827 (2003).

[40] J. S. Williams, Rep. Prog. Phys. **49**, 491 (1986).

[41] F. Wooten, K. Winer, and D. Weaire, Phys. Rev. Lett. **54**, 1392 (1985).

[42] J. S. Custer, M. O. Thompson, D. C. Jacobson, J. M. Poate, S. Roorda, and W. C. Sinke, Appl. Phys. Lett. **64**, 437 (1994).